Metals and Materials International (2020) 26:1562–1573
https://doi.org/10.1007/s12540-019-00416-x

Advanced Approach to Modify Friction Stir Spot Welding Process

Behrouz Bagheri[1] · Mahmoud Abbasi[2] · Amin Abdollahzadeh[1,3] · Hamid Omidvar[1]

Received: 22 April 2019 / Accepted: 30 July 2019 / Published online: 28 August 2019

Abstract
Nowadays, friction stir spot welding (FSSW) is used in automotive, rail vehicle construction, the aerospace industry, and electrical industry. In the current research, a modified version of the FSSW process entitled friction stir spot vibration welding was introduced to join Al5083 specimens. The joining specimens were vibrated normal to the tool movement direction, while the joint position cooled by passing coolant through the fixture. Different characteristics of developed joint namely microstructure, mechanical properties, corrosion behavior were studied. The results showed that stir zone grain size decreased significantly as the vibration was employed and the joint position was cooled. It was found that vibration enhanced the dynamic recrystallization and coolant decreased the grain growth. Both led to enhanced grain refinement in the stir zone. The results also indicated that shear strength and hardness of the weld region increased as the modified version of FSSW was applied. Corrosion tests revealed that corrosion resistance increased as the modified method was applied.

Keywords Friction stir spot welding · Vibration · Coolant · Microstructure · Corrosion

List of Symbols

FSSW	Friction stir spot welding
FSSVW	Friction stir spot vibration welding
BM	Base metal
WN	Weld nugget
SZ	Stir zone
EBSD	Electron backscatter diffraction
TEM	Transmission electron microscopy
SEM	Scanning electron microscopy
TMAZ	Thermo-mechanical affected zone
HAZ	Heat-affected zone
SEM	Scanning electron microscopy
UFSW	Underwater friction stir welding
SFSW	Submerged friction stir welding
TC	Thermo-couple
VMM	Vision measuring machine
I_{corr}	Corrosion current density
E_{corr}	Corrosion potential
C.R	Corrosion rate
R_p	Polarization resistance
NAMLT	Nitric acid mass loss test
IGC	Intergranular corrosion

✉ Behrouz Bagheri
b.bagheri@aut.ac.ir

[1] Department of Mining and Metallurgy, Amirkabir University of Technology, Tehran, Iran

[2] Faculty of Engineering, University of Kashan, Kashan, Iran

[3] Department of Materials Science and Engineering, Sharif University of Technology, Tehran, Iran

1 Introduction

Friction stir spot welding (FSSW) is known as a solid-state joining process to weld structural components in different configurations [1–5]. It has been originated from friction stir welding (FSW). FSSW has been utilized to replace conventional spot welding methods to reduce joining steps and lower costs in different industries [6, 7]. Tool in FSSW, unlike the FSW method, is not traversed and the joint is obtained by forcibly plunging a rotating tool into the joining sheets in the lap joint until the shoulder is in contact with the surface of the top sheet. The frictional heat, due to contact between the tool and workpiece, softens the material around the tool, so that the material is stirred and the sheets bond together metallurgically without melting. After a short dwell time, the tool is pulled out of the sheets. Presence of keyhole in the middle of the joint is a characteristic of an FSSW joint [8].

FSSW morphology is described by four different areas including parent or base metal (BM), thermo-mechanically affected zone (TMAZ), heat affected zone (HAZ), and stir zone (SZ) or weld nugget (WN) in which a heavily deformed

material is created [9–11]. The quality of the weld area depends on different factors such as dwelling time, rotation speed, plunging depth, shoulder and pin shape, material flow around the pin.

Ravi Sekhar et al. [12] studied the effect of tool rotation speed on shear fracture load of FSS (friction stir spot) welded AA5052-H38 aluminum alloy. They found that with the increase in tool rotational speed up to a constant value the shear fracture load increases and a further increase in the speed, decreases the shear fracture load. Jedrasiak et al. [13] presented an FE (finite model) thermal model for modeling the thermal histories of joining specimens during FSSW. Their model successfully predicted the thermal histories for similar and dissimilar alloy joints during FSSW. D'Urso and Giardini [14] evaluated the effects of rotational speed, axial feed rate and plunging depth on temperature distribution and the mechanical properties of the FSSW lap joints on AA7050 aluminum alloy plates. The effects of FSSW process parameters on mechanical properties of joint were investigated by Yuan et al. [15]. They varied tool rotation speed and plunge depth to find the effects of these parameters on lap-shear separation load. They observed three different weld separation modes under lap-shear loading: interfacial separation, nugget fracture separation, and upper sheet fracture separation. They also found that there was no direct relationship between microhardness distribution and separation location. Zhang et al. [16] investigated the effect of welding parameters on mechanical properties of AA5052 joint during FSSW. They found that rotation speed influences joint strength while dwell time doesn't have any effect.

Various trials have been carried out to modify the FSSW to increase the mechanical properties of the joint. Refill FSSW [17], pin-less FSSW [18] and swing FSSW [19] are some of these modifications presented to eliminate the keyhole. Wu et al. [20] developed a liquid-nitrogen cooling FSSW (C-FSSW) technology for joining AZ31 magnesium alloy sheets. They found that the grain size of the stir zone and HAZ of C-FSS welded joint were smaller than that of FSS welded joint and the tensile shear load of the former joint was larger than that of the latter joint. Rostamiyan et al. [21] mixed two welding methods, including FSSW, and ultrasonic welding to improve the weld quality. In their research, FSSW was performed by ultrasonic vibration of the tool. They examined the impact of process parameters namely vibration, tool rotary speed, tool plunge depth, and dwell time on mechanical properties such as lap-shear force and hardness. They reported that the introduction of vibration enhanced the lap shear force and hardness. Ji et al. [22] introduced the "ultrasonic-assisted friction stir spot welding" (UAFSSW) technique. They employed this process to join dissimilar AZ31 and AA6061alloy sheets. They showed that ultrasonic vibration was significant for the upward material flow of the bottom plate and to get a flawless joint. They also found that the existence of ultrasonic vibration improved the stir zone width and led to finer grains in the stir zone.

In this work, a new modified method of FSSW was introduced. In this method, entitled FSSVW, stir motion of tool was accompanied by workpiece vibration. To increase the efficiency of this method, the joint position was also cooled. The effects of workpiece vibration and presence of coolant on mechanical properties namely hardness, lap shear strength as well as microstructural characteristics of Al5083 joint were investigated. The effects of these variables on corrosion properties of joint were also studied.

2 Materials and Methods

AA5083 aluminum alloy sheets with 2 and 0.7 mm thicknesses were used as joining materials. The chemical composition of the studied sheets is presented in Table 1. Specimens with a size of 100 mm × 25 mm were prepared from the sheets. The specimens were cleared of oil and any debris and finally, they were cleaned by ethanol. Various FSSW methods namely, conventional FSSW, FSSVW, FSSW + coolant, and FSSVW + coolant were applied to join the specimens. The specimens were fixed in the fixture in lap situation while the thick specimen was on top and the overlap distance was the same for all conditions and it was 25 mm.

All welding methods were carried out by the milling machine. For conventional FSSW and FSSW + coolant processes, the fixture was installed on the milling machine table, while for FSSVW and FSSVW + coolant, the fixture was installed on a special machine designed to provide workpiece vibration during FSSW. The machine works based on a camshaft mechanism. The motor shaft rotation is transformed into the linear and reciprocating movement of a vibrating plate through a camshaft. Vibration amplitude is designed to be 0.5 mm. Vibration frequency is adjusted by motor shaft rotation speed which is controlled by a driver. The vibration frequency in the current research was 50 Hz. Schematic design of machine designed and manufactured for FSSVW is presented in Fig. 1a. For welding conditions accompanied by coolant, the fixture with a hole in it for passing the circulating coolant beneath the joint position was used. Schematic design of this fixture is presented in Fig. 1b.

Table 1 Chemical composition of the studied AA5083 aluminium alloy sheet (wt%)

Al	Fe	Si	Mn	Cr	Cu	Mg
Balance	0.4	0.5	0.4	0.25	0.1	5.1

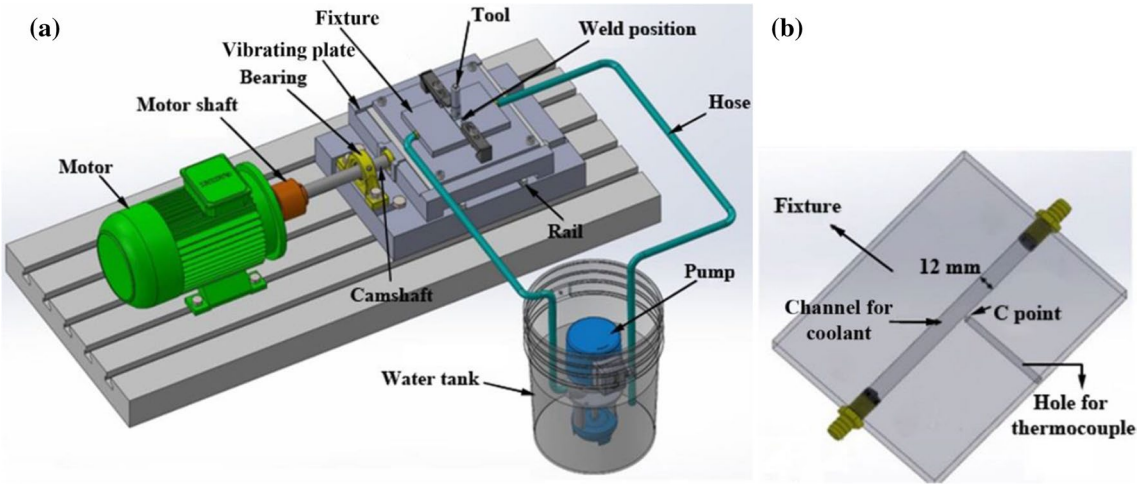

Fig. 1 **a** Schematic design of machine manufactured for FSSVW with the application of coolant, **b** design of the fixture

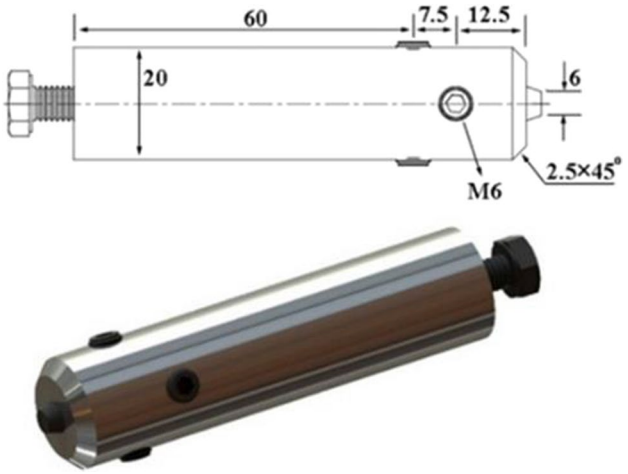

Fig. 2 Schematic design of tool used for welding processes (all dimensions are in mm)

A hole was cut in the fixture to place K-type thermocouple and to measure the temperature variations around the joint during the welding conditions (Fig. 1b). The thermocouple measures the temperature of a constant point (point C) around the weld area.

A two-pieces tool consisting of a cylindrical shoulder from M2 steel with a hardness of 65 HRC and a trapezoidal cylinder pin from WC was utilized for welding processes. Schematic view of the tool is presented in Fig. 2. Based on trial and error method, optimum welding parameters were chosen. For all welding conditions, the rotation speed was 1200 rpm and dwell time was 10 s.

Metallography techniques based on ASTM E3-11 [23] were utilized to reveal the microstructure. A solution of 12 ml HNO3, 15 ml HF, 128 ml H2O, and 45 ml HCL was used as the etchant. Linear intercept method based on ASTM E112-13 [24] was used to get the stir zone grain size of welded specimens. Scanning electron microscopy (SEM) equipped with electron backscatter diffraction (EBSD) and transmission electron microscopy (TEM) were used to characterize the microstructure and analyze the grains and their crystallographic orientation. EBSD specimens were electro-polished in a solution of 85 ml C2H5OH and 15 ml HClO4 at 6 V for 10–15 s. TEM specimens were prepared by double-jet electrolytic polishing using a solution of 75 ml CH3OH and 25 ml HNO3 at 250 K under a potential of 15 V.

The mechanical properties of welded specimens were examined by tensile shear tests. Figure 3 presents the shape of the test pieces utilized for tensile shear tests. Tensile shear tests were performed at ambient temperature with a cross-head speed of 0.5 mm/min. Vickers microhardness test based on ASTM E384-17 [25] was applied to measure the hardness of welded specimens. During hardness testing, load and dwell time were 100 gf and 10 s, respectively.

To study the corrosion behavior of the welded specimens, electrochemical impedance spectroscopy (EIS) and polarization techniques were used. The tests were performed on the cross-section of the welded specimens using an Autolab potentio/galvanostat while the same surface area (15 mm^2) was used for all specimens. Before the tests, the surfaces of the samples were polished to reach the same roughness and then cleaned in acetone. The samples were immersed in 3.5 wt% NaCl solution for 10 min to reach an almost constant open circuit potential (OCP) and then were polarized with a scan rate of 1 mV/s in a potential range of − 200 mV to + 500 mV versus OCP. The counter and reference electrodes were platinum wire and Ag/AgCl, respectively. The corrosion current density of the samples was obtained using Tafel extrapolation method. EIS tests were performed in a

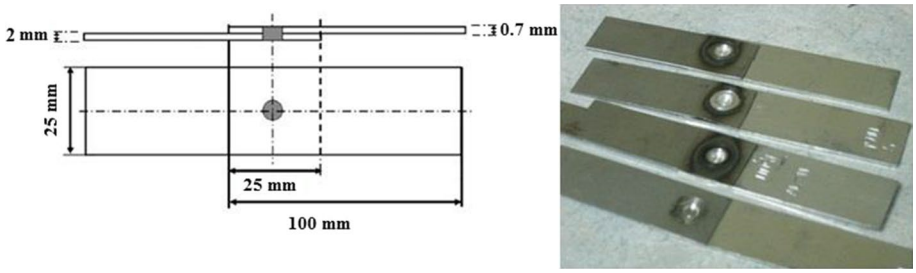

Fig. 3 Specimen configuration for the tensile shear test

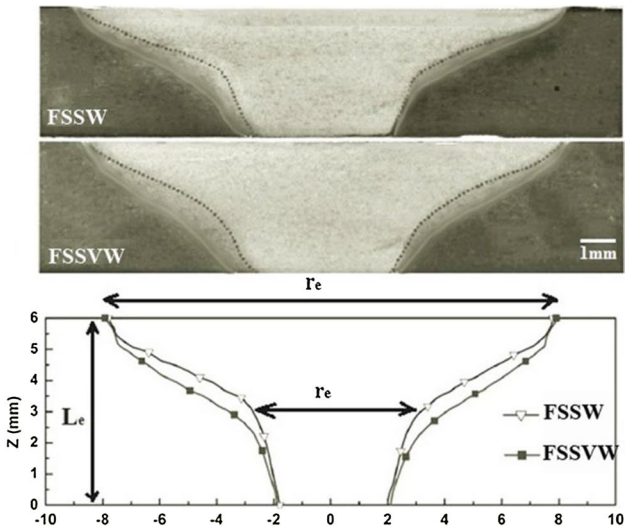

Fig. 4 View macrograph of the welded zones for FSS and FSSV welded specimens

frequency range from 100 kHz to 10 MHz with a voltage amplitude of 20 mV in the OCP.

3 Results and Discussion

3.1 Macrostructure Analysis

Figure 4 presents the cross-section macrostructure of FSS and FSSV welded specimens. No cracks or porosities are visible in these sections. It is observed that the stir zone for FSSV welded specimen is larger than that in FSS welded specimens. The workpiece vibration is the reason for stir zone enlargement.

3.2 Microstructure Analysis

Microstructures of different zones of the studied FSS and FSSV welded specimens are shown in Fig. 5. It is observed that for each specimen, the smallest grains relate to the stir zones and the stir zone grains of FSSV welded specimen with coolant are smaller than those of other specimens.

Dynamic recrystallization is known as the main mechanism for grain refinement during FSW and FSSW [26, 27]. During FSW, the heat generated due to contact between tool and workpiece softens the material around the tool and the tool rotation results in the material deformation. Plastic deformation increases the dislocation density in the material [28]. High temperature during straining leads to dislocation movement and dynamic recovery (DR) and correspondingly, low angle grain boundaries (LABs) with a misorientation angle less than 15º develop within the main grain boundaries. Arrangement of dislocations to form LABs is presented in Fig. 6a. As straining proceeds, misorientation between sub-grains increases and high angle grain boundaries (HABs), which behave as main grain boundaries, develop (DRX) and as a result, finer grains are developed [29]. Constitution of a new boundary (HAB) within the main grain and development of fine grain is presented in Fig. 6b.

The authors believe that the presence of vibration enhances the material straining during the welding process and results in more DRX and correspondingly finer grains are developed. The EBSD maps of different zones for the studied welding conditions are observed in Fig. 7. Grains for FSSV welded specimens are smaller than grains for FSS welded specimens. The misorientation angle histograms of the studied welded specimens are observed in Fig. 8. According to Fig. 8, for the FSSV welded specimens the fraction of high-angle grain boundaries (misorientation angle > 15) is larger than that in the FSS welded specimens. As noted before, the reason might be the occurrence of more DRX in FSSV welded specimens which results in finer grains. As grain size decreases, the volume content of grain boundaries with high misorientation angle increases.

It is also clear in Fig. 7 that application of coolant during FSSW and FSSVW processes leads to more refined grains and based on Fig. 8, specimens welded with the application of coolant have a higher content of HABs. Presence of coolant decreases the temperature and impedes the grain growth. It has been found that high temperature during FSW and FSSW processes results in grain growth [26]. Stir zone grain size values for the studied specimens are presented in Table 2.

The effect of the presence of vibration and coolant during FSSW process can also be explained through the

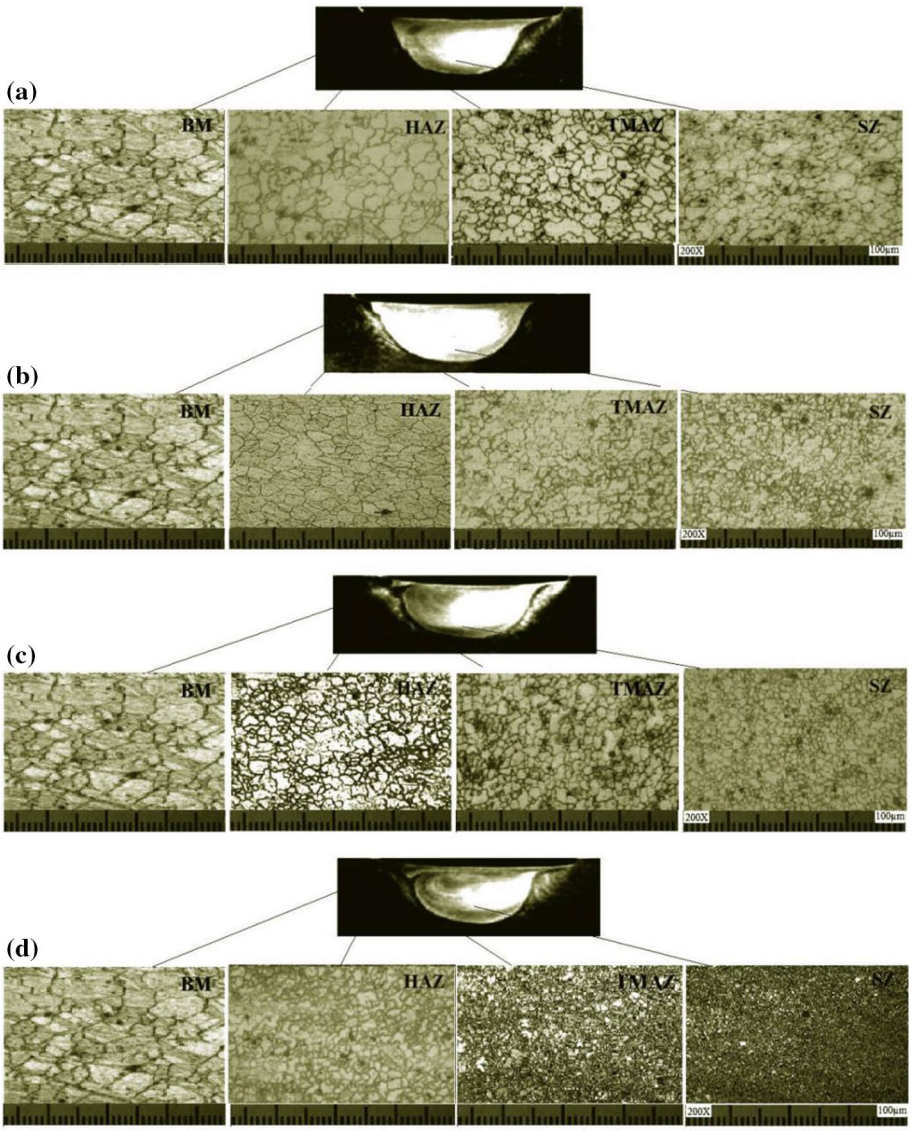

Fig. 5 Microstructures of welded areas for the specimens relating to the studied welding conditions, **a** FSSW, **b** FSSVW, **c** FSSW + coolant, and **d** FSSVW + coolant

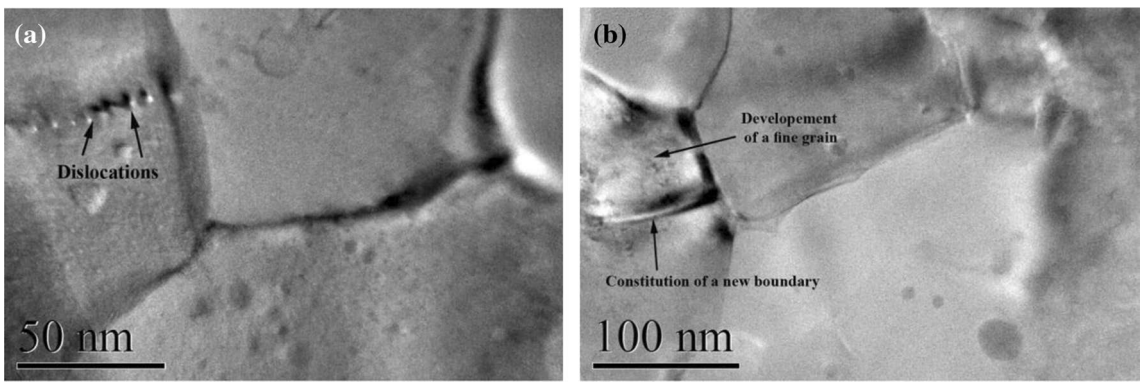

Fig. 6 **a** Arrangement of dislocations to form LAB and **b** constitution of new boundaries (HAB) within the main grain boundaries and development of fine grain

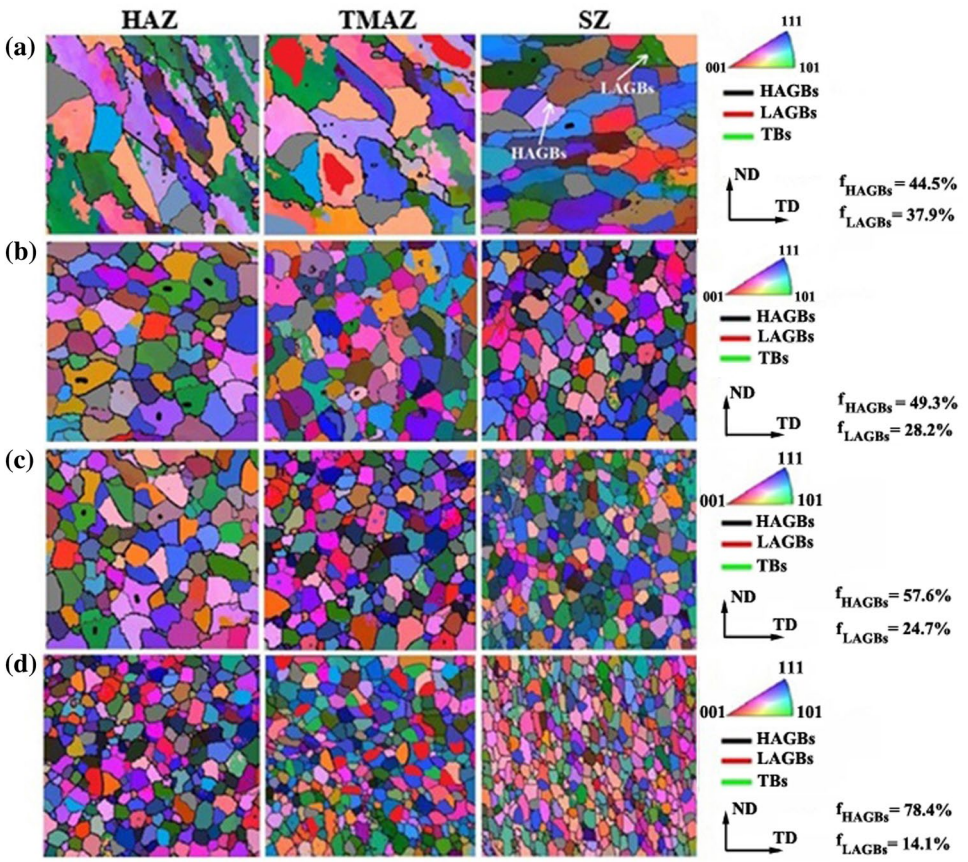

Fig. 7 EBSD maps of welded areas for the specimens relating to the studied welding conditions, **a** FSSW, **b** FSSVW, **c** FSSW + coolant, and **d** FSSVW + coolant

Zener-Hollomon (Z) parameter. Z parameter is used to describe the combined effect of strain rate and temperature on plastic deformation and is given by [30]:

$$Z = \dot{\epsilon} \exp\left(\frac{Q}{RT}\right) \tag{1}$$

where $\dot{\epsilon}$ is the strain rate, T is the deformation temperature, Q and R are the activation energy and the gas constant, respectively. Moreover, the relation between the Z parameter and grain size (d) is presented by the following relation [31]:

$$d^{-1} = a \ln Z - b \tag{2}$$

Which a and b are constants. According to Eq. 2, d decreases as the Z parameter increases. As vibration is applied during FSSW, due to accompanying of workpiece vibration with stirring motion of material around the tool, more strain and strain rate is applied on material [32]. On the other hand, the presence of coolant during FSSW decreases the temperature. High strain rate and low temperature both result in high Z parameter (Eq. 1) and according to Eq. 2, low size grains develop.

The temperature history of point C (Fig. 1b) for different welding conditions is presented in Fig. 9. It is observed that for all welding conditions, the temperature first increases and then decreases and there is a maximum point for each graph. According to Fig. 9, the maximum temperature relating to FSSVW process is the highest and the maximum temperature relating to FSSW process with the application of coolant is the lowest. This indicates that workpiece vibration during FSSW enhances the temperature around the joint and application of coolant during FSSW decreases the temperature; although, the effect of coolant is higher than the effect of vibration. As vibration is applied, the material around the joint is strained more and correspondingly more work hardening is applied on the material and additionally, the friction between the tool and the workpiece enhances [32]. In this regard, workpiece vibration during FSSW process leads to temperature increase.

3.3 Tensile Shear Strength Analysis

Tensile shear strength-displacement curves of the studied specimens are presented in Fig. 10. It is observed in Fig. 10 that the shear strength of FSSV welded specimen is higher than that relating to FSS welded specimen and presence of coolant during welding increases the strength. These can be related to the effect of microstructure. It was observed (Fig. 7) that not only the presence of vibration but also the application of coolant during FSSW decrease the grain size. As grain size decreases, the volume content

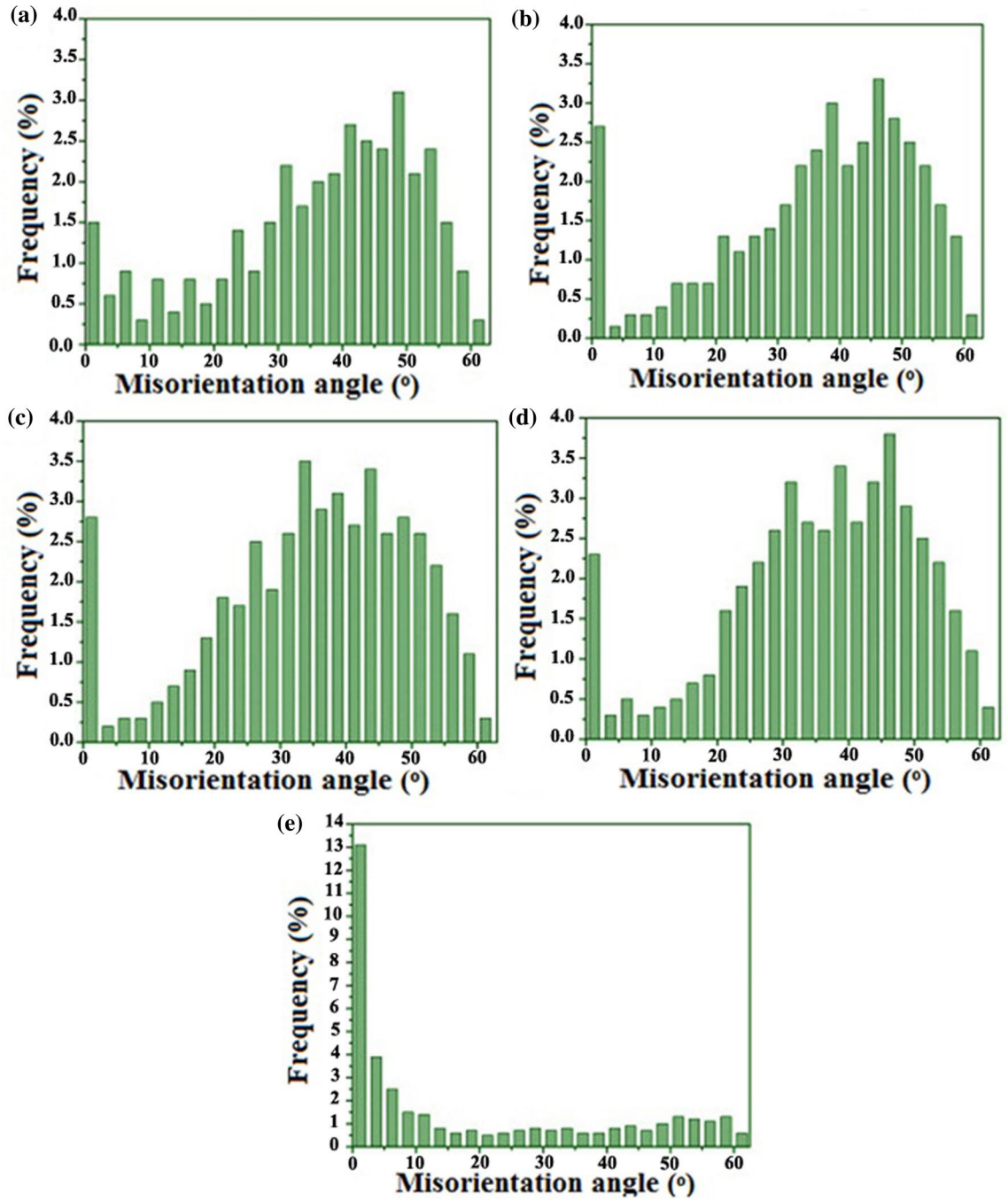

Fig. 8 Misorientation angle histograms for the specimens relating to the studied welding conditions, **a** FSSW, **b** FSSVW, **c** FSSW + coolant, **d** FSSVW + coolant and **e** base metal

of grain boundaries increases. Grain boundaries decrease the movement of dislocations and increase strength [33]. According to Hall–Petch equation ($\sigma = \sigma_i + kd^{-\frac{1}{2}}$) [34], strength (σ) increases as grain size (d) decreases. It is interesting to note that in Fig. 11 the strength of FSS welded specimen with the application of coolant is higher than the strength of FSSV welded specimen. This indicates that the effect of the application of coolant on strength is higher than the presence of vibration. Table 2 showed that the grain size of the former specimen is lower than the latter specimen. The lower grain size results in higher strength.

Table 2 The values of grain size for base material and stir zones of welded specimens

Specimen	Grain size (μm)
Base metal	64 ± 2
FSSW	39 ± 2
FSSVW	27 ± 2
FSSW + coolant	15 ± 2
FSSVW + coolant	9 ± 2

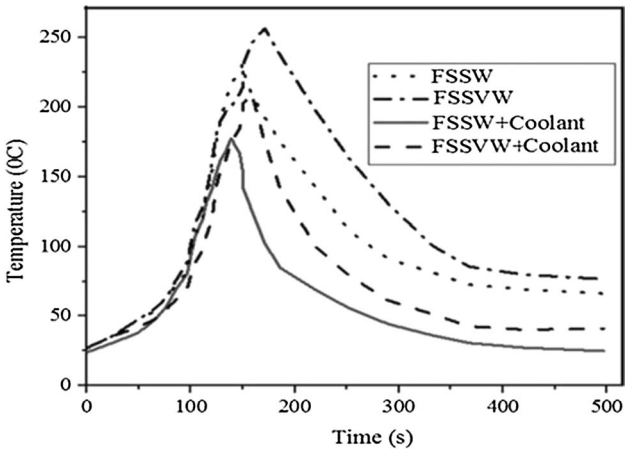

Fig. 9 Temperature history of point C of the fixture (Fig. 1b) relating to the different welding conditions

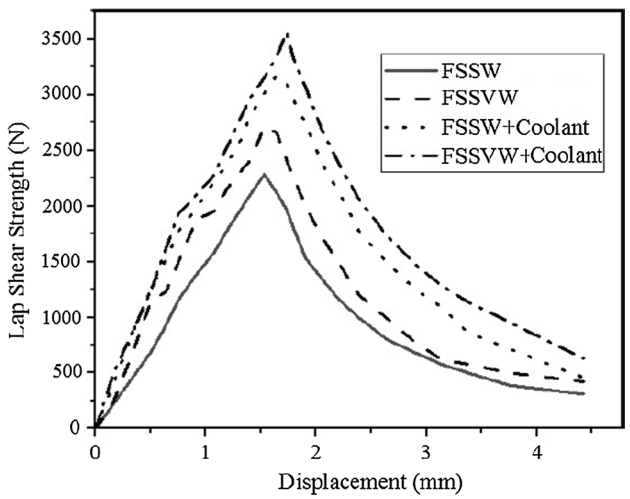

Fig. 10 The effect of the presence of vibration and coolant during FSSW on tensile shear strength of welded specimens

3.4 Fracture Surface Analysis

Figure 11 shows the scanning electron microscopy (SEM) images of fracture surfaces of the studied specimens. Dimples which are characteristic of ductile fracture surfaces [34] are observed in these surfaces. Ductile fracture is characterized by large amounts of plastic deformation [35]. During deformation, dislocations move and their density increases. At early stages of deformation, the dislocations glide freely, but during straining the dislocations intersect with each other and some jogs or barriers are formed [36]. These jogs or barriers are initial sites for the formation of voids; however, inclusions and secondary phase particles are other preferable sites for void formation [36]. As straining proceeds, voids coalescence and form small cracks. The cracks grow and finally fracture occurs. The voids are responsible for the constitution of dimples in fracture surface and metals with the more ductility have a smaller size of voids [37].

According to Fig. 11 the fracture surfaces of the studied specimens are porous and the size of voids for FSSV welded specimen with the application of coolant is the lowest. This agrees well with the results presented in Fig. 10 which shows that displacement at maximum shear stress for the noted specimen is the highest.

3.5 Hardness analysis

The hardness maps of the studied specimens relating to weld cross-section are presented in Fig. 12. It is observed that hardness values of the stir zones for the studied specimens are higher than other zones. Figure 12 also shows that hardness values of FSSV welded specimen are higher than those relating to FSS welded specimen and application of coolant increases the hardness. These can be related to the effect of microstructure. According to Hall–Petch equation [34], strength and hardness increase as grain size decreases. As grain size decreases, the barriers for movement of dislocation increase and the hardness increases. It was observed (Fig. 7) that grains of stir zones due to the occurrence of DRX were smaller than other areas and the stir zone grain size decreased with the application of coolant. Figure 7 also indicated that stir zone grain size decreased as workpiece vibration was applied.

Higher hardness of base metal with respect to weld zones (Fig. 12) may be related to the development of residual stresses in weld zones. Delijaicov et al. [37] found that longitudinal tensile residual stresses develop in weld zones and decrease the hardness of weld zones with respect to base metals.

Figure 13 presents the hardness distribution curves of the welded specimens. Data relates to different zones of the welded specimens namely stir zone (SZ), thermo-mechanically affected zone (TMAZ), and heat-affected zone (HAZ). It observed that the hardness values relating to stirring zones due to smaller grain size are higher than

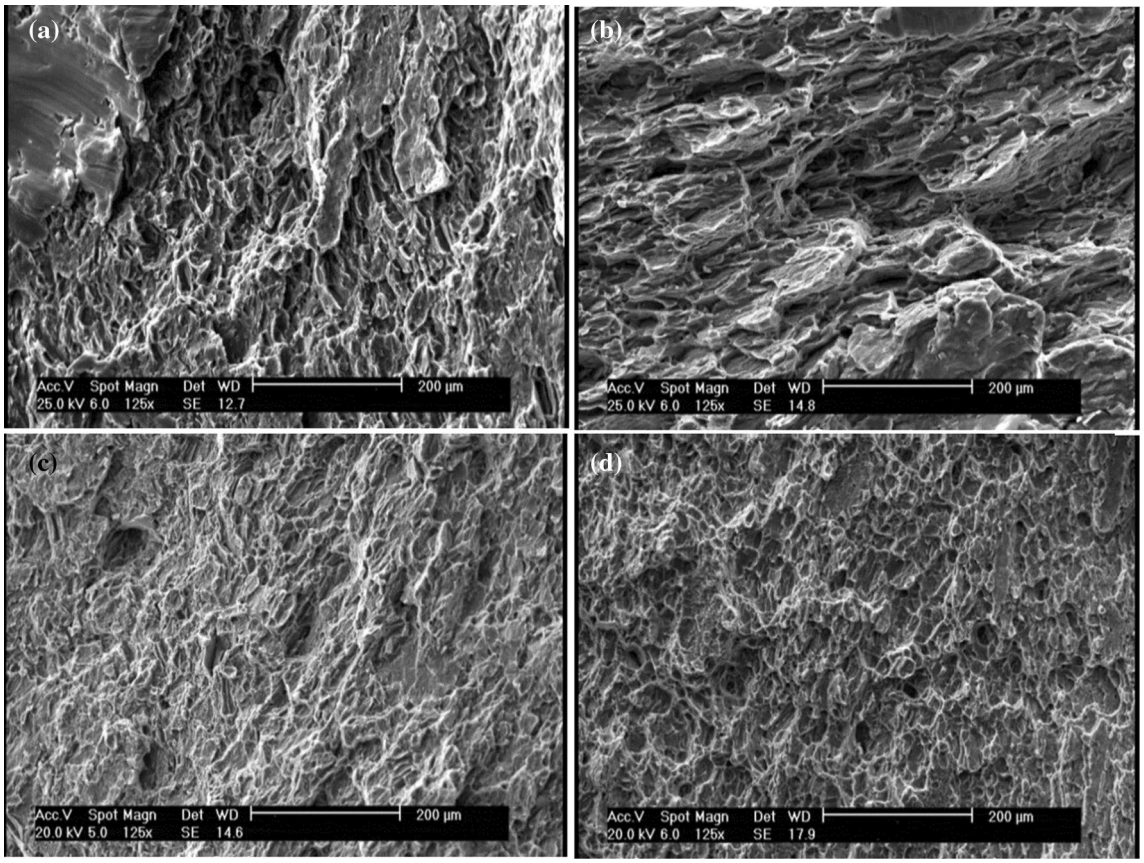

Fig. 11 Fracture surfaces of the studied specimens relating to the different welding conditions, **a** FSSW, **b** FSSVW, **c** FSSW + coolant, and **d** FSSVW + coolant

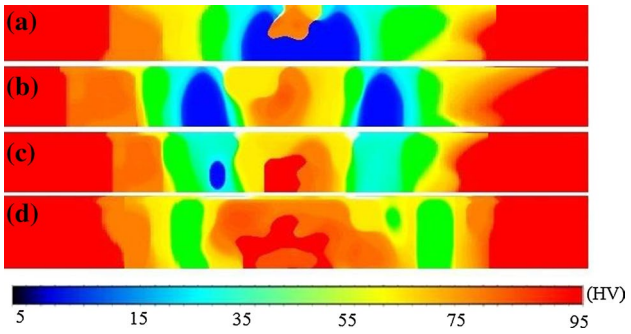

Fig. 12 View of weld cross-section hardness maps of the studied specimens, **a** FSSW, **b** FSSVW, **c** FSSW + coolant, and **d** FSSVW + coolant

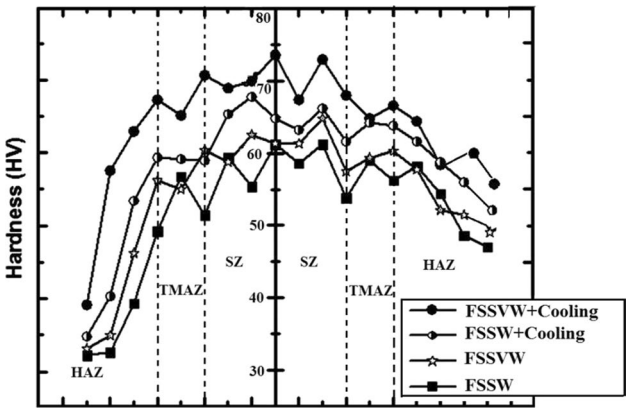

Fig. 13 Hardness distribution of weld cross-section for different welding conditions

those values relating to other areas for different welding conditions.

3.6 Corrosion Behavior

It has been known that the corrosion properties of AA5083 alloy depend on microstructure and the amount and distribution of intermetallic particles such as Al_3Mg_2 (β-phase) [38]. These particles precipitate along with the segregation of magnesium at grain boundaries. Grain boundaries and intermetallic particles numerate as preferable sites for corrosion initiation [39].

Corrosion behavior of the studied specimens was analyzed by utilizing the polarization and Nyquist diagrams.

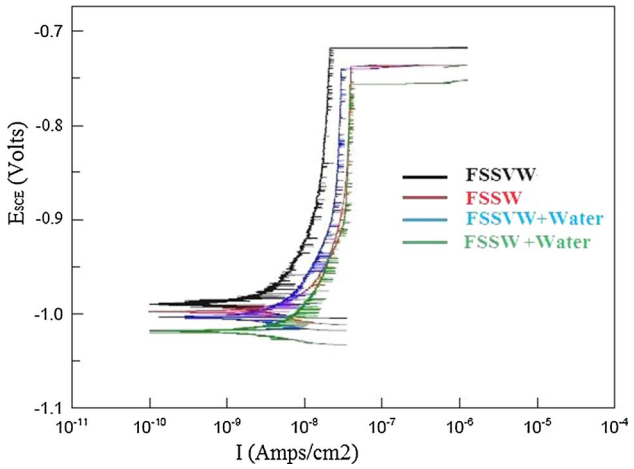

Fig. 14 Anodic polarization curves for various welding conditions

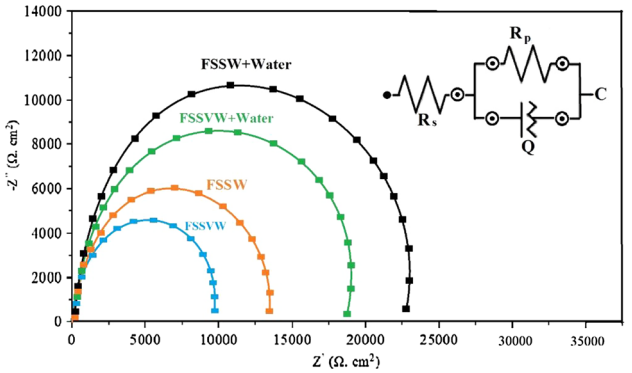

Fig. 15 Nyquist curves of the studied specimens relating to different welding conditions

Table 3 Corrosion rates of the studied specimens

Welding method	E_{corr} (mV) vs.SCE	I_{crro} (μA/cm^2)	Corrosion rate (mpy)
FSSVW	−732	2.80	1.23
FSSW	−715	1.50	0.85
FSSVW + water	−703	1.26	0.56
FSSW + water	−685	1.15	0.48

Table 4 Polarization resistance values of the studied specimens relating to different welding conditions

Welding condition	FSSW	FSSVW	FSSW + coolant	FSSVW + coolant
R_p (Ω cm^2)	13,200	9800	22,700	18,800

The Polarization curves of the studied specimens are presented in Fig. 14. Using the Tafel extrapolation method, corrosion rates of different specimens were obtained. Corrosion rates of the studied specimens are presented in Table 3.

According to Table 4, the corrosion rates of welded specimens with the application of coolant are lower than those of other specimens and the corrosion rate of FSSV welded specimen is higher than that of FSS welded specimen. These results can be related to the effects of microstructure and the presence of intermetallic particles. As stated before, grain boundaries and secondary particles decrease the corrosion resistance [39]. Additionally, the detrimental effect of the secondary particles on corrosion resistance increases as particles size enhances [40]. Gharavi et al. [41] noted that intermetallic particles size increases as the temperature during FSW increases. Presence of water as the coolant, during FSSW and FSSVW processes, decreases the temperature and impedes the growth of intermetallic particles. Therefore, the intermetallic particles are small and the corrosion rate is low. Application of coolant not only decreases the grain size (Fig. 7) but also decreases the intermetallic particles size. The former effect increases the corrosion rate and the latter one decreases the corrosion rate. Based on results in Table 4, it seems that the effect of intermetallic particles size on corrosion rate is higher than the effect of grain boundaries. So, the application of water as a coolant during FSSW is recommended. On the other hand, workpiece vibration during FSSVW process enhances the DRX and leads to more refined grains with higher volume content of grain boundaries. The relationship between the corrosion rate (i_{corr}) and grain size (d) for a wide range of metals is given by [42]:

$$i_{corr} = \alpha + \beta(d)^{-0.5} \tag{3}$$

where α and β are constants. According to Eq. 3, the corrosion rate increases as grain size decreases [37]. So, a higher corrosion rate of FSSV welded specimen with respect to FSS welded specimen is predictable. Based on results presented in Table 4, in FSSW process, application of water as coolant for enhancement of corrosion resistance is good but, workpiece vibration is not good. The interesting point to note in Table 4 is the condition of simultaneous application of coolant and vibration during FSSW. The results show that the effect of coolant on corrosion resistance is higher than the vibration.

Figure 15 presents the Nyquist semicircles of different studied specimens. These semicircles confirm the results obtained using polarization curves. According to the Stern–Geary equation (Eq. 4) [43], the corrosion current density and, therefore, the corrosion rate is inversely related to the polarization resistance. So, the corrosion rate increases as polarization resistance decreases.

$$i_{corr} = \frac{\beta_a \beta_c}{2.3R_p(\beta_a + \beta_c)'} \tag{4}$$

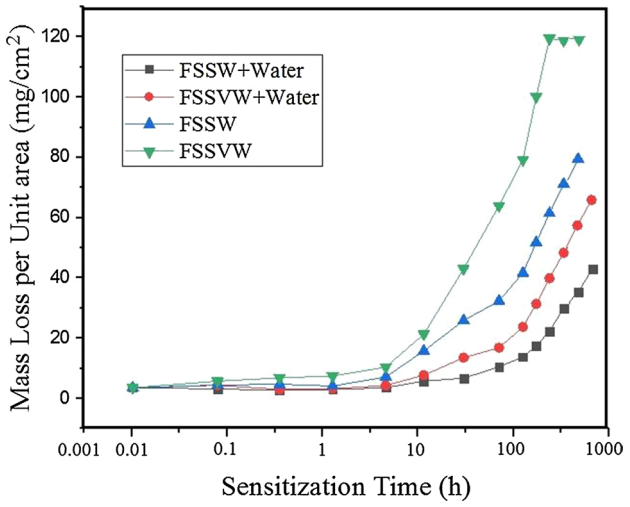

Fig. 16 Influence of sensitization time on the intergranular corrosion susceptibility of the studied specimens relating to different welding conditions

In Eq. 4, i_{corr} is the corrosion current density, R_p is the polarization resistance of the specimen and β_a and β_c are the anodic and cathodic Tafel slopes, respectively. A simple equivalent circuit is shown in Fig. 15 was used to calculate the polarization resistance of the specimens. The measured values for the studied specimens are presented in Table 4. According to Table 4, the highest polarization resistance belongs to FSS welded specimen with the application of coolant and the lowest one relates to FSSV welded specimen. Therefore, according to Eq. 4, the highest corrosion resistance is predicted for FSS welded specimen with the application of coolant which agrees well with data in Table 3. Considering the EIS and polarization results, it could be concluded that the workpiece vibration decreases the corrosion resistance and application of coolant during FSSW increases it.

The influence of sensitization on the intergranular corrosion (IGC) susceptibility of different welded specimens at 150 °C was studied. The results are presented in Fig. 16. It can be seen that the sensitivity of various welded specimens to IGC increases with increasing time at a given condition. It is observed in Fig. 16 that FSS welded specimen with the application of coolant has the lowest values of mass loss.

4 Conclusion

In the current research, a new method was presented to modify the FSSW process and to join AA5083 alloy specimens. Joining specimens were vibrated during FSSW and the joint position was cooled by water as the coolant. The results showed this new method, compared to conventional FSSW, increased the shear strength and hardness of the joint and additionally, increased the corrosion resistance of joint. It was concluded that:

1. Workpiece vibration led to grain refinement in the stir zone. This was related to enhanced DRX as the vibration was applied.
2. Application of coolant during FSSW decreases the temperature. This impedes the grain growth and intermetallic particle enlargement. Application of coolant increases the strength and corrosion resistance of the joint.
3. Compared to conventional FSSW, simultaneous application of coolant and workpiece vibration during FSSW enhanced the corrosion resistance of joint.
4. Application of this new method as a modified version of FSSW is recommended.

References

1. A. Addison, A. Robelou, Friction stir spot welding: principal parameters and their efects, in *Proc. 5th International Friction Stir Welding Symposium*, TWI Ltd. Metz, France, (2004)
2. M M. Awang, V. Mucino, Z. Feng, S. David, Thermomechanical modeling of friction stir spot welding (FSSW) process: use of an explicit adaptive meshing scheme, 2nd *SAE Congress*, SAE Warrendale, USA (2005)
3. M. Awang, V.H. Mucino, Energy generation during friction stir spot welding (FSSW) of Al 6061-T6 plates. J. Mater. Manuf. Proc. **25**(1), 167 (2010)
4. S. Babu, V. Sanka, G. JanakiRam, P. Venkitakrishnan, G. MadhusudhanReddy, K. PrasadRao, Microstructures and mechanical properties of friction stir spot welded aluminum alloy AA2014. J. Mater. Eng. Perform **22**, 1–14 (2012)
5. H. Badarinarayan, Q. Yang, S. Zhu, Effect of tool geometry on static strength of friction stir spot-welded aluminum alloy. Int. J. Mach. Tool. Manuf. **49**(2), 142 (2009)
6. D. Bakavos, P.B. Prangnell, Effect of reduced or zero pin length and anvil insulation on friction stir spot welding thin gauge 6111 automotive sheet. Sci. Technol. Weld. Join **14**, 443 (2009)
7. D. Bakavos, F. Haddadi, P. Prangnell, FSSW of aluminium automotive sheet (private communication) (2009)
8. D. Bakavos, Y. Chen, L. Babout, P. Prangnell, Material interactions in a novel pinless tool approach to friction stir spot welding thin aluminum sheet. Metall. Metal. Trans. A. **42**, 1266 (2011)
9. D. Mitlin, V. Radmilovic, T. Pan, Z. Feng, M. Santella, Structure-properties relations in spot friction welded 6111 T4 aluminum, in *TMS Annual Meeeting*, San Francisco (2005)
10. B. Bagheri, A.A. M. Rizi, M. Abbasi, M. Givi, Friction stir spot vibration welding: improving the microstructure and mechanical properties of Al5083 joint, in *Metallography, Microstructure, and Analysis* (2019)
11. R. Hancock, Friction welding of Aluminum Cuts Energy Cost by 99%. Weld. J **83**, 40 (2004)
12. S. RaviSekhar, V. Chittaranjandas, D. Govardhan, R. Karthikeyan, Effect of tool rotation speed on friction stir spot welded AA5052-H38 aluminum alloy. Mater. Today Proc. **5**, 5536–5543 (2018)

13. P. Jedrasiak, Thermal modeling of Al-Al and Al-steel friction stir spot welding. J. Mater. Eng. Perform **25**, 4089–4098 (2016)
14. G. D'Urso, C. Giardini, Thermo-mechanical characterization of friction stir spot welded AA7050 sheets by menas of experimental and FEM analyses. Mater **9**, 689–703 (2016)
15. W. Yuan, R.S. Mishra, S. Webb, Effect of tool design and process parameters on properties of Al alloy 6016 friction stir spot welds. J. Mater. Proc. Technol **211**(6), 972–977 (2012)
16. Z.H. Zhang, X.Q. Yang, J.L. Zhang, G. Zhou, X. Xu, B. Zou, Effect of welding parameters on microstructure and mechanical properties of friction stir spot welded 5052 aluminum alloy. Mater. Des. **32**(8–9), 4461–4470 (2011)
17. T. Rosendo, B. Parra, M.A.D. Tier, Mechanical and microstructural investigation of friction spot welded AA6181-T4 aluminium alloy. Mater. Des. **32**, 1094–1100 (2011)
18. Y. Tozaki, Y. Uematsu, K. Tokaji, A newly developed tool without probe for friction stir spot welding and its performance. J. Mater. Proc. Technol. **210**, 844–851 (2010)
19. Y. Fang, *The Research on the Processes and Proprerties of Pinless Friction Stir Spot Welding* (Jiangsu University of Science and Technology, Jiangsu, 2009)
20. D. Wu, J. Shen, M.B. Zhou, L. Cheng, J.X. Sang, Development of liquid-nitrogen-cooling friction stir spot welding for AZ31 magnesium alloy joints. Int. J. Miner. Metall. Mater. **24**, 1169–1176 (2017)
21. Y. Rostamiyan, A. Seidanloo, H. Sohrabpoor, R. Teimouri, Experimental studies on ultrasonically assisted friction stir spot welding of AA6061. Arch. Civil. Mech. Eng **15**, 335–346 (2015)
22. S.D. Ji, Z.W. Li, Y.M. Yue, S.S. Gao, Investigation of ultrasonic assited friction stir spot welding of magnesium alloy to aluminum alloy. Strenght Mater **48**, 2–7 (2016)
23. ASTM-E3-11, *Standard Guide for Preparation of Metallographic Specimens. Annual Book of ASTM Standards*, vol. 3.01 (American Society for Testing and Materials, West Conshohocken, 2017)
24. ASTM-E112-13, *Standard Test Methods for Determining Average Grain Size. Annual Book of ASTM Standards*, vol. 3.01 (American Society for Testing and Materials, West Conshohocken, 2017)
25. ASTM-E8M, *Standard Test Methods for Tension Testing of Metallic Material. Annual Book of ASTM Standards*, vol. 3.01 (American Society for Testing and Materials, West Conshohocken, 2016)
26. A. Rosochowski, *Severe Plastic Deformation Technology* (Whittles Publishing, Scoland, 2017), pp. 138–141
27. M. Abbasi, M. Givi, A. Ramazani, Friction stir vibration processing: A new method to improve the microstructure and mechanical properties of Al5052/SiC surface nano-composite layer. Int. J. Adv. Manuf. Technol. **100**, 1463–1473 (2019)
28. G.E. Dieter, D. Bacon, *Mechanical and Metallurgy* (McGraw-Hill, London, 1988), pp. 184–193
29. J.Q. Su, T.W. Nelson, C.J. Sterling, Microstructure evolution during FSW/FSP of high strength aluminum alloys. Mater. Sci. Eng. A. **405**, 277–286 (2005)
30. M. Rahmi, M. Abbasi, Friction stir vibration welding process: modified version of friction stir welding process. Int. J. Adv. Manuf. Technol. **90**, 141–151 (2017)
31. C.I. Chang, C.J. Lee, J.C. Huang, Relationship between grain size and Zener–Holloman parameter during friction stir processing in AZ31 Mg alloys. Scr. Mater. **51**, 509–514 (2008)
32. O. Barooni, M. Abbasi, M. Givi, B. Bagheri, New method to improve the microstructure and mechanical properties of joint obtained using FSW. Int. J. Adv. Manuf. Technol. **93**, 4371–4378 (2017)
33. A. Abdollahzadeh, A. Shokuhfar, J.M. Cabrera, A.P. Zhilyaev, H. Omidvar, In-situ nanocomposite in friction stir welding of 6061-T6 aluminum alloy to AZ31 magnesium alloy. J. Mater. Proc. Technol. **263**, 296–307 (2019)
34. B. Bagheri, M. Abbasi, M. Givi, Effects of vibration on microstructure and thermal properties of friction stir spot welded (FSSW) aluminum alloy (Al5083). Int. J. Precis. Eng. Manuf. (2019). https://doi.org/10.1007/s12541-019-00134-9
35. V. Uthaisangsuk, Microstructure based formability modeling of multiphase steels. Ph. D. Thesis, IEHK, RWTH- Aachen (2009)
36. D. Hull, D.J. Bacon, *Introduction to Dislocations* (Butterworth-Heinemann, Britain, 2011), pp. 87–95
37. S. Delijaicov, P.A.D.O. Silva, H.B. Resende, M.H.F. Batalha, Effect of weld parameters on residual stress, hardness and microstructure of dissimilar AA2024-T3 and AA7475-T761 friction stir welded joints. Mater. Res. **21**, 1–11 (2018)
38. A.E. Coy, F. Viejo, F.G. Garcia, Z. Liu, P. Skeldon, G.E. Thompson, Effect of excimer laser surface melting on the microstructure and corrosion performance of the die cast AZ91D magnesium alloy. Corros. Sci. **52**, 387–397 (2010)
39. J. Corral, E.A. Trillo, Y. Li, L.E. Murr, Corrosion of friction-stir welded aluminum alloys 2024 and 2195. J. Mater. Sci. Lett. **19**, 2117–2122 (2000)
40. M.G. Fontana, *Corrosion Engineering* (McGraw-Hill, London, 1985), pp. 112–121
41. F. Gharavi, K.H.A. Matoria, R. Yunus, N.K. Othman, Investigation of the nugget zone corrosion behavior in friction stir welded lap joints of 6061-T6 aluminum alloy. Mater. Res. **17**(6), 1563–1574 (2014)
42. K.D. Ralston, N. Birbilis, C.H.J. Davies, Revealing the relationship between grain size and corrosion rate of metals. Scr. Mater. **63**(12), 1201–1204 (2010)
43. U. Angest, M. Buchler, On the applicability of the Stern–Geary relationship to determine instaneous corrosion rates in macro-cell corrosion. Mater. Corros. **66**, 1017–1028 (2015)